Electronic Supplementary Material (ESI) for Journal of Materials Chemistry C.

Supporting Information

Scalable realization of conductive graphene films for high-efficiency microwave antennas

T. T. Tung[a(†)], S. J. Chen[b(†)], C. Fumeaux[b(*)] and D. Losic[a(*)]

(a) School of Chemical engineering, the University of Adelaide, Adelaide, 5005 North Terrace, South Australia

(b) School of Electrical and Electronic Engineering, the University of Adelaide, Adelaide, 5005 North Terrace, South Australia

(†) T. T. Tung and S. J. Chen contributed equally

(*) Corresponding to: Prof. Christophe Fumeaux and Prof. Dusan Losic

Experimental details

1. Materials and Chemicals

Graphite flakes from the Uley graphite mine (Australia) and expanded graphite were kindly supplied by Valence Industries, South Australia. Potassium permanganate ($KMnO_4$) was purchased from Sigma-Aldrich, Australia. Sulphuric acid (H_2SO_4, 98%), phosphoric acid (H_3PO_4, 85% w/w), hydrogen peroxide (H_2O_2, 30%), hydrochloric acid (HCl, 35%) were purchased from Chem-Supply, Australia. All chemicals were used directly without further processing.

2. Exfoliation of graphene and preparation of graphene conductive films

Graphene was prepared by liquid phase exfoliation of expanded graphite (EG) in graphene oxide (GO) aqueous suspension, in which GO was prepared by the modified Hummer's method as reported previously[1]. Briefly, for processing GO-mediated exfoliation of graphene from EG, 300 mg EG powders and 300 mL water were added in a 500 mL capped-round bottom flask, pre-sonicated with bath sonicator for 1 h, and then 100 mL GO suspension with concentration of 1mg/mL was added. The mixture was subjected to sonicate with a UIP1000hd (Hielscher) with sonotrode (diameter of 22 mm) at a power of 200 W, and amplitude of 80% for 10 h where the temperature was kept less than 40 ˚C. Subsequently, the as-prepared suspension was left to stand for 1 day for setting down the large graphite particles, and the supernatant was extracted by centrifugation at 4200 rpm for 1 h, which led to the graphene being separated from the complex and precipitated in the GO supernatant. The graphene product was decanted, washed several times with water, and redispersed in water to make

graphene inks with a concentration of 1 mg/mL. In order to make graphene film, the as-received graphene ink was filtered through a Teflon membrane with diameter of 0.45 µm. It was then dried in a convection oven at 60 ˚C for 5 h, and peeled off carefully from the filter paper. Finally, the film was subjected for thermal annealing at 900 ˚C under Ar atmosphere for 1 h, and cooled down slowly under the same environment.

3. Characterization of materials

Scanning electron microscopy (SEM) images were recorded using a Quanta 450 instrument operated at an acceleration voltage of 20 kV and an emission current of 10 mA. Transmission electron microscopy (TEM) was conducted on a TECNAI 20 microscope operated at 120 kV. X-ray photoelectron spectroscopy (XPS) measurements were performed with ESCA2000 (VG Microtech) system using a monochromatizedaluminum Kα anode. The Raman mapping spectra were recorded using DXR^{TM}xiRaman Imaging Microscope. Spectra were recorded over the range of 500 - 4000 cm^{-1} with an excitation wavelength of 532 nm. The X-ray diffraction (XRD) (Model Miniflex 600, Rigaku, Japan) measurement was performed from 2θ = 5 – 80° to illuminate the composition of the graphene product at a scan rate of 5°/min. The surface resistance was obtained using a CMT series JANDEL four-point probe at room temperature in which a current of 10 µA was applied, and a non-contact sheet resistance tester from SURAGUS GmbH - EddyCus® TF lab 2020 as well. The conductivity was calculated by the following equation:

$$\sigma = \frac{1}{t.Rs} \qquad \text{(S - 1)}$$

where *Rs* is the sheet resistance; *t* is the thin film thickness measured by using a HITACHI SU1510 SEM (Japan).

Figure S1. Shows the TEM image of GO-adsorbed onto graphene surface (Fis S1a), this physical interaction however can be easily desorbed under radiation of electrons beam (Fig S1b,c). After removal GO by using centrifugation at high speed, the TEM image shows high polycrystallinity and very stable under the same radiation condition.

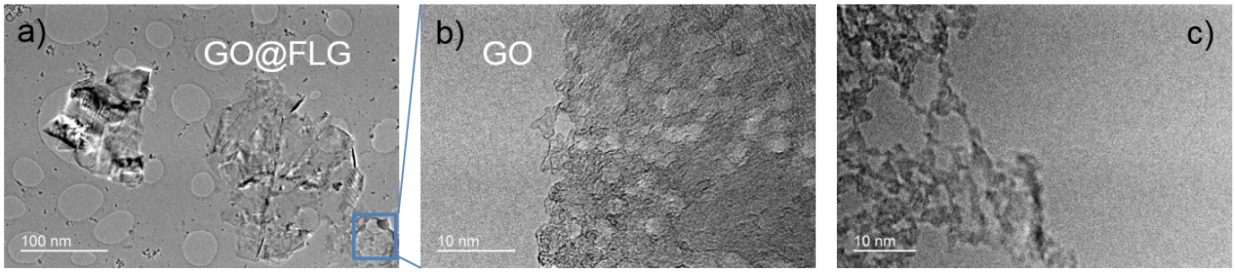

Figure S1. TEM images of (a) GO-FLG complex, (b and c) desorbed GO under radiation of electrons beam

The thickness of graphene sheets of the graphene production was confirmed by redispersed graphene powders in in isopropanol with an assistance of sonicator and deposited on silicon wafer under spin coating for further characterization by using AFM. As can be seen in Figure S2, the average thickness of graphene sheets is about 2 nm, this is consistent with Raman analysis.

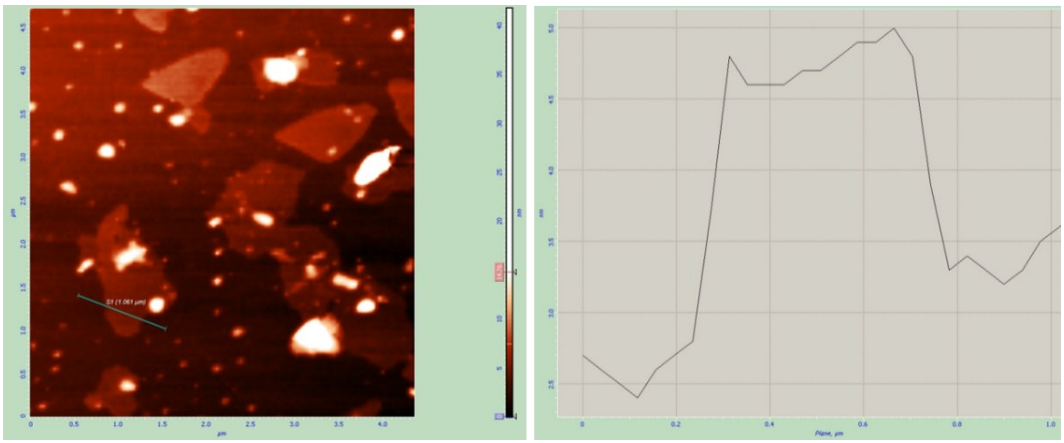

Figure S2. AFM image of graphene production with average thickness of 2 nm

Raman spectroscopy was studied for characterizing the thickness and structural changes of different materials including expanded graphite (precursor), GO (mediator) and graphene (product) (as can be seen in the Figure S3). While the Raman spectrum shows three typical graphene bands: D-band (sp^3 defects), G-band (tangential vibration of sp^2 carbon atoms) and 2D-band (the second order of D band). A comparison of the intensity ratio of D and G band (I_D/I_G) for GO, graphene and expanded graphite are 0.78, 0.124 and 0.09, respectively. Moreover, it is known that the 2D band position and the shape corresponds to the specific numbers of stacked graphene films. The band splitting of 2 D band from single to multiple layer arises from lowering symmetry that take place when number of graphene layer increases. As compared to expanded graphite, the 2D peak positions in graphene/FLG shifted considerably to a lower wavenumber by 24 cm^{-1}, from 2712 to 2688 cm^{-1}, the peak is symmetric and its intensity is higher than that of graphite precursor (Fig. 3, right side), The distinct band shape is suggesting a successful exfoliation to less than 6 layers graphene in the production as referenced. [2-5]. Based on accepted criteria for graphene material with less< 10 graphene layers is considered as graphene and with >10 layer as graphite so we are confident that our prepared material is graphene.

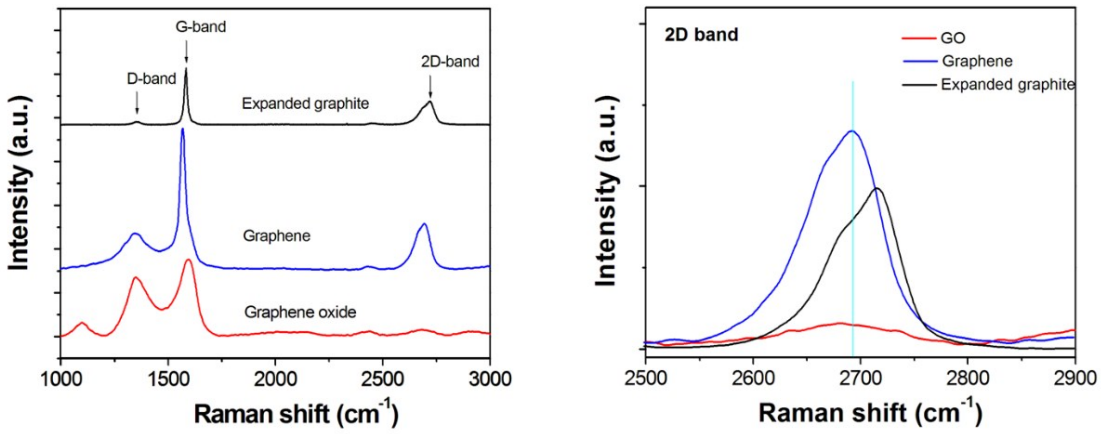

Figure S3. A comparative Raman spectra of Graphene production versus EG (precursor) and GO (mediator)

4. Design, fabrication and measurement of antenna

UWB technology is very promising for wireless communication systems, since its wide frequency band signals offer high data rate while a very low power level is needed when compared with conventional narrowband technologies. Therefore, as a critical component of the technology, UWB antenna designs have been receiving considerable attention. In this work, an UWB antenna based on the graphene film (as showed in Fig. S1), with operational frequency from 3.1 to 10.6 GHz (band specified by |S11| < 10 dB), is designed with a full-wave 3-D electromagnetic simulation tool CST Microwave Studio 2015 (CST).

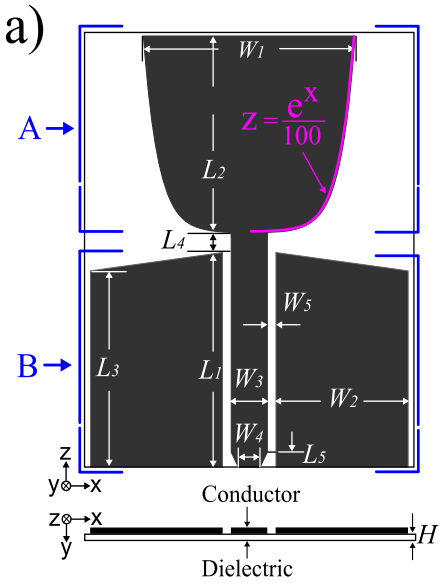

Figure S4. A new designed UWB antenna based on graphene film

Table S1. Antenna dimensions

Dimensions [mm]	L1	L2	L3	L4	L5	W1	W2	W3	W4	W5	H
	14.0	13.8	12.8	1.2	1.0	14.3	9.0	2.5	2.0	0.5	0.07

Antenna design: The antenna configuration and dimensions are depicted in Fig. S4 and Table 1, respectively. The antenna comprises an exponentially tapered block on the top section (denoted as A in Fig. S4) and a coplanar waveguide (CPW) feeding structure at the bottom section (denoted as B in Fig. S4). These two sections, A and B, operate together as radiator with a predominately vertical linear polarization. The broadband antenna performance is achieved through the smooth antenna intrinsic impedance transition from the feed to free space, which is formed by the two exponentially tapered edges of A and the two top edges of B. One of the most important parameters in the antenna design is CPW dimensions with center conductor width *W3* and slot width *W5,* since it determines the CPW characteristic impedance which influences the antenna matching (|S11|), and the induced current density along the CPW slots which is proportional to the conduction losses. The later factor is more importantly in this case, as the graphene film conductivity is relatively low which can lead to much higher conduction losses and consequently a lower antenna efficiency when *W5* is very small. Thus the optimized value of *W5* yields a satisfactory antenna matching (with the corresponding *W3* dimension for impedance matching) and a maximum antenna efficiency.

Graphene conductivity and film thickness: Since the overall graphene thin film thickness significantly influences the antenna efficiency, an investigation based on CST is performed. The conductivity of the graphene film is assumed to be constant in the microwave frequency range, and therefore the ac-sheet resistance can be retrieved from the dc-conductivity using equation (S-1) under consideration of the Skin effect. Additionally, the surface roughness (with standard deviation of around 10 μm) is factored into the calculation of the frequency-dependent sheet impedance of the sample. The simulation results are shown in Fig. S5 where simulated antenna radiation efficiencies are plotted against the corresponding graphene thin film thickness at 3.1, 6.0 and 10.6 GHz. As the graphene thin film thickness increases from 4 to 130 μm, the antenna radiation efficiency rises with diminishing return, that is, after a rapid initial increase, the efficiency stabilizes to its achievable maximum at around 100 μm. Further increase of the layer does not provide significant efficiency increase in the

considered frequency range. This demonstrates that a sufficient graphene thin film thickness is very critical for achieving satisfactory antenna efficiency.

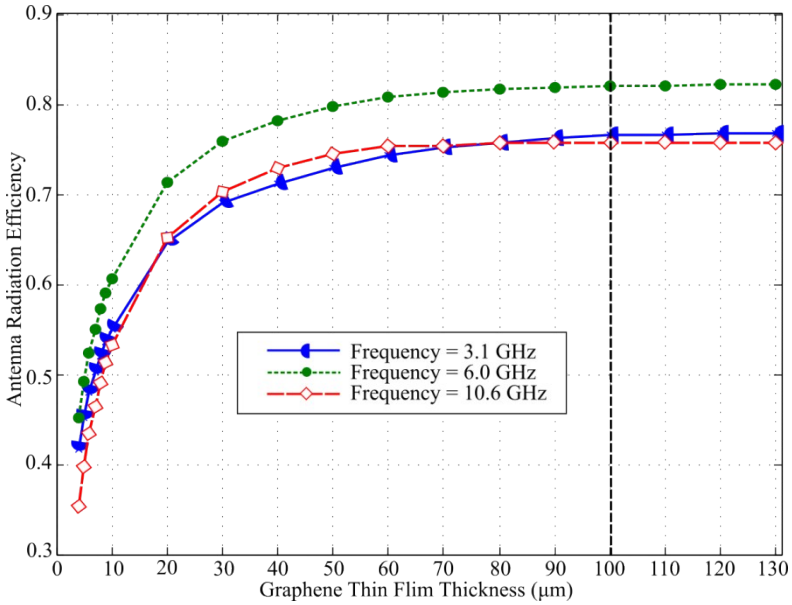

Figure S5. Antenna radiation efficiency with different graphene thin film thickness at 3.1, 6.0 and 10.6 GHz

Fabrication: In order to achieve accurate patterning, a laser milling machine was used. A transparent substrate based on adhesive tape was used, since it is transparent to the laser beam and thus can be kept intact during milling. Moreover, it provides robust mechanical support and physical isolation for the antenna. The 100-μm-thick adhesive tape has a relative permittivity of $\varepsilon = 3$ and loss tangent $\tan\delta = 0.01$ both estimated based on fitted values in simulation. Firstly, the graphene film was attached to a piece of adhesive tape, and placed into the laser milling machine, then the laser cutting beam was swept on the film with a programmed path by which all redundant graphene film was vaporized to define the geometry of the antenna. Secondly, the antenna was adhered to another piece of adhesive tape, which has a rectangular notch trimmed at the bottom of the CPW to leave space for electrical connection of a SMA (SubMiniature version A) connector. Thirdly, conductive epoxy (Circuit works CW2400) was applied between the SMA connector and the antenna CPW to realize an excellent electrical connection. Finally, a very thin layer of non–conductive epoxy was coated on top of the conductive silver pain to provide a secure mechanical bond.

Measurements: To verify the antenna performance, reflection coefficient, radiation patterns, conduction efficiency and radiation efficiency were experimentally characterized in the anechoic

chamber of the University of Adelaide. An identical antenna made of copper was realized and its performance was measured as a reference.

Reference

1. *D. N. H. Tran, S. Kabiri and D. Losic.* Carbon 76 (2014) 193-202
2. *J. Rafiee et al. Nature Mater. 2012, 11, 217-222*
3. *Y. Hernandez et al. Nature Nanotech. 2008, 3, 563-568*
4. *A.C. Ferrari et al. Phys. Rev. Lett. 2006, 97, 187401-1-4*
5. *A.C. Ferrari et al. Nature Nanotech. 2013, 8, 235-243.*